Lawrence Berkeley National Laboratory

Title

Visual Comfort Analysis of Innovative Interior and Exterior Shading Systems for Commercial Buildings using High Resolution Luminance Images

Permalink

https://escholarship.org/uc/item/4458d0t8

Author

Konis, Kyle

Publication Date

2011-03-01

Visual Comfort Analysis of Innovative Interior and Exterior Shading Systems for Commercial Buildings using High Resolution Luminance Images

Kyle Konis
Lawrence Berkeley National Laboratory

Eleanor Lee
Lawrence Berkeley National Labortory

Robert Clear
Lawrence Berkeley National Laboratory

January 2011

DISCLAIMER

Visual Comfort Analysis of Innovative Interior and Exterior Shading Systems for Commercial Buildings using High Resolution Luminance Images

K.Konis, E.S.Lee, R.D.Clear, Ph.D

Building Technologies Program, Environmental Energy Technologies Division, Lawrence Berkeley National Laboratory, Mailstop 90-3111, 1 Cyclotron Road, Berkeley, CA 94720, USA

Abstract

The objective of this study was to explore how calibrated high dynamic range (HDR) images (luminance maps) acquired in real world daylit environments can be used to characterize, evaluate, and compare visual comfort conditions of innovative facade shading and light-redirecting systems. Detailed (1536 x 1536 pixel) luminance maps were time-lapse acquired from two view positions in an unoccupied full scale testbed facility. These maps were analyzed using existing visual comfort metrics to quantify how innovative interior and exterior shading systems compare to conventional systems under real sun and sky conditions over a solstice-to-solstice test interval. The results provide a case study in the challenges and potential of methods of visualizing, evaluating and summarizing daily and seasonal variation of visual comfort conditions computed from large sets of image data.

Keywords: daylighting, high dynamic range imaging, discomfort glare.

1. Introduction

In recent years, mainstream acceptance of the "green building movement" has led to the construction of a significant number of buildings with highly glazed facades, designed with the dual goals of 1) complying with green building certification programs (e.g., LEED daylight and view credits) and 2) the reduction of electrical lighting energy consumption via daylighting. Casual inspection of these buildings in operation often reveals that shading systems are routinely deployed by occupants to maintain comfortable visual conditions, reducing the potential for lighting energy reduction as well as visual connection to the exterior.

This study focuses on evaluating the visual comfort conditions produced from a number of innovative interior and exterior facade shading and light-redirecting systems that have the potential to more effectively balance the goals of visual comfort with daylight transmission in comparison to conventional shading systems (e.g., manually operated Venetian blinds or roller shades) used in typical sidelit perimeter zones. In this study, the term "innovative" refers to systems that employ one or more of the following strategies: sub-division of the window wall into an upper daylighting zone and a lower "view" zone, optical light redirection, translucent materials, and automation of slat angle and/or height adjustment.

Prior to the availability of luminance maps to assess lighting conditions in real spaces, the limitations of available photometric monitoring equipment (e.g., shielded illuminance sensors, spot luminance meters) resulted in simplified methods of glare assessment in daylit spaces. Average luminances of large window areas using shielded sensors have commonly been used to compute the daylight glare index (DGI) [IEA SHC

Task 21, 2000] as well as numerous other discomfort glare indices. In addition, average luminances from shielded sensors have been correlated to subjective response data in the derivation of a predictive model that relates the average luminance of the entire window to the probability of the shade being lowered [Clear et al. 2006].

The primary limitation of these methods is that the boundary of the glare source must be pre-defined. This is a problem in daylit spaces because the boundary and position of glare sources are constantly changing. An additional limitation is that a physical shield must be fabricated with a profile identical to the desired target. This presents a challenge when defining targets with irregular profiles, such as the boundary between the landscape and the sky as viewed through the window. A final limitation is that each pre-defined region requires an individual illuminance sensor, restricting the number of glare sources that can be defined for practical reasons, often leading to the entire window being defined as a single (and very large) glare source. Because the DGI is sensitive to both the size and position of each glare source, the definition of the entire window as a single source can lead to misleading results.

HDR images store luminance data on a "per-pixel" scale, providing far greater resolution for visual comfort analysis, enabling both the definition and analysis of an arbitrary number of pre-defined regions, and the possibility of detecting glare sources throughout the full field of view to compute any number of discomfort glare metrics. In computer graphics, the original HDR format (*Radiance* RGBE) was developed for the lighting simulation engine *Radiance* in order to record the photometric conditions of synthetic lighting environments [Ward 1991, 1994]. In following years, techniques were developed to produce HDR images from real-world scenes [Debevec 1997, Mitsunaga & Nayar 1999] by compositing multiple, exposure-bracketed, low dynamic range (LDR) images (e.g., JPEG) into a single HDR image. Motivated by the possibility of using HDR in real spaces for photometric analysis, methods are now available to produce calibrated HDR images, commonly referred to as luminance maps [Inanici & Galvin, 2004]. Wienold and Christoffersen [2006] derived a new daylight glare prediction model based on HDR data correlated to subjective response.

In this study, two methods of visual comfort analysis using luminance maps are demonstrated on a variety of interior and exterior shading systems, some with reflective surfaces, some with automated controls, and some where the window wall is subdivided into an upper and lower region. These systems have been designed to more effectively balance the competing goals of admitting useful daylight without the associated glare. The Illuminating Engineering Society of North America (IESNA) recommended contrast ratio limits and Hopkinson Cornell Large Source Glare Index (DGI)[1] are used as a basis for evaluation. The analysis focuses on addressing two questions: Do existing metrics and summary indices computed from luminance maps enable differentiation between systems? And, what value can time-lapse imaging add over more conventional methods of visual comfort assessment?

2. Measurements and procedures

2.1. Test facility

Experimental tests were conducted in the 88.4 m^2 (952 ft^2) Advanced Windows Testbed Facility located at the Lawrence Berkeley National Laboratory (LBNL) in Berkeley, California (latitude 37°4'N, longitude 122°1'W). The facility consists of three identical side-by-side test rooms (Figure 1) built to represent a commercial office environment and were unoccupied during this study. Testing was conducted with electric lighting on and dimmed to maintain a setpoint illuminance of 538 lux at the workplane.

---

[1] We did not use the Wienold and Christoffersen's glare prediction model due to an error in the software tool at the time, which prevented analysis of our HDR images.
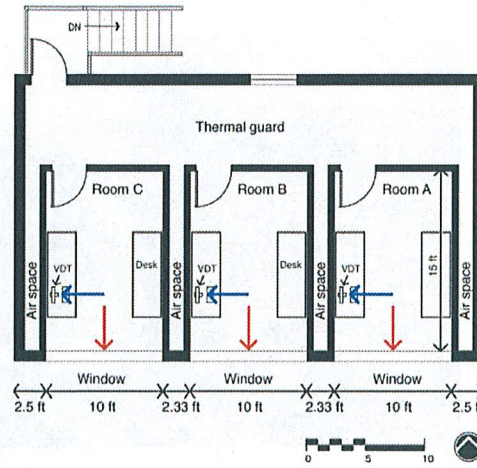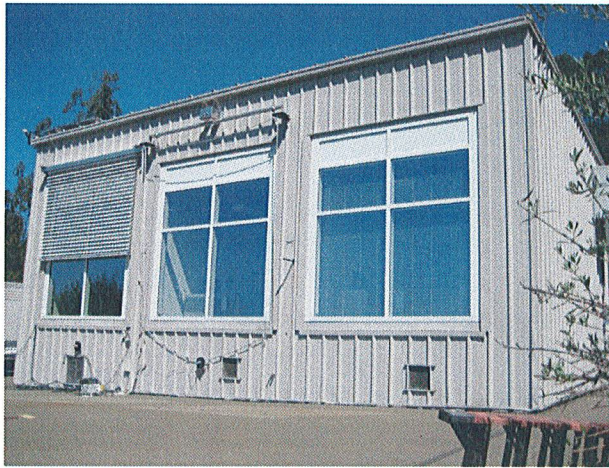
Figure 1. Exterior view of the south-facing facade of the Advanced Windows Testbed Facility (left) and floor plan indicating view positions of HDR measurements in each test room (right).

2.2. Acquisition of HDR Images

Images were taken vertically at two locations within each room assuming a seated occupant (1.2 m (4 ft) eye height): a) looking at the west sidewall and computer monitor or visual display terminal (VDT) 1.52 m (5 ft) from the window and b) normal and centered on the window, 1.2 m (4 ft) from the window (Figure 1). Images were acquired from 6 AM to 6 PM Standard Time and therefore some data include non-daylit conditions.

Each HDR image was composited from a set of nine, 1536 x 1536 pixel, LDR images, exposure-bracketed in 1 EV steps using conventional CCD cameras (Nikon 990) with an equidistant fisheye lens (Nikon fc e8, 183°). Compositing was achieved using the program *hdrgen,* which converts the RGB pixel values of exposure bracketed LDR images into real-world luminances [Mitsunaga & Nayar 1999]. Automation of acquisition and exposure bracketing was achieved using a series of scripts written for this application. A more general script (HDRcapOSX) was written later for the higher quality Canon EOS 5D digital camera series for a related project, which was then ported and tested on the Mac OS X 10.5.8 operating system by [Fan and Mardaljevic 2009]. This script is backwards compatible to OSX 10.4.x and available free at: (http://www.iesd.dmu.ac.uk/~jm/doku.php?id=resources:hdrcaposx).

2.3. Post-processing of HDR images

To correct for the light fall off typical of wide-angle camera systems, a "digital filter" was applied to each HDR image as a post-process in *Radiance* using the method developed by Inanici & Galvin [2004]. During the time required to acquire a bracketed set of images (~1 minute), the luminous environment is rarely stable and large swings in outdoor sky conditions can introduce significant measurement errors. To control for unstable lighting conditions, the global vertical illuminance computed from the image was compared to the average of two readings from an adjacent vertical illuminance sensor (type=Licor LI-210, cosine-corrected, nominal accuracy = 3%, range = 0 - 15,000 lux): immediately before and after acquisition of the bracketed set of images (Figure 3). The image was then uniformly scaled by adjusting the *exposure* line of the image file header so that the global vertical illuminance computed from the image matched the average of the two illuminance readings.
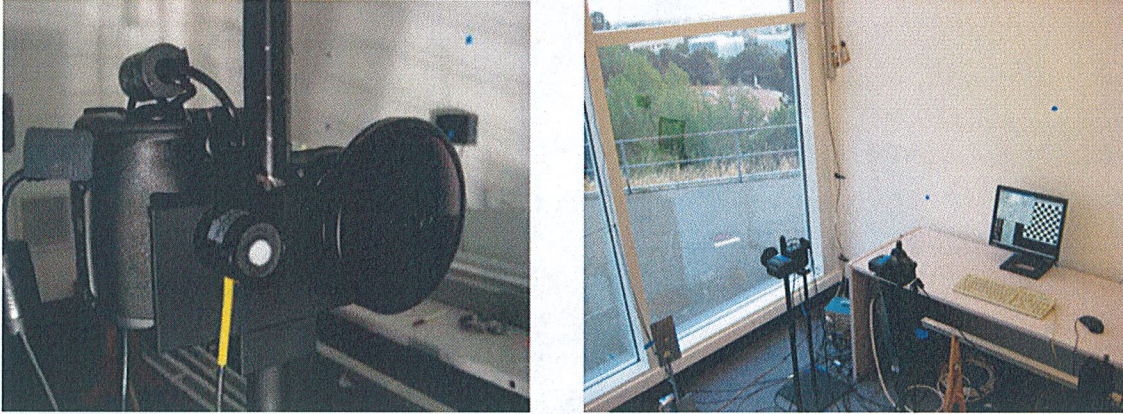
Figure 3. Image of typical Nikon 990 camera setup with the adjacent vertical illuminance sensor used in calibration of HDR luminance maps (left) and overview of position and orientation of cameras in a test room (right).

2.4. Measurement Errors

To quantify errors associated with changes in vertical illuminance during acquisition, a test was performed to examine the accuracy of luminance maps under dynamic sky conditions. The camera was positioned adjacent to a shielded luminance sensor. A mask was defined for the luminance maps that matched the field of view of the shielded sensor (Figure 5). The average luminance computed from the luminance map was then compared to the shielded sensor and reported in terms of percent error and magnitude error. Figure 7 presents data for one of the six cameras tested. Each of the six cameras was tested for one day resulting in a total of ~144 images per camera (867 images total). During this test, the average luminance of the masked region ranged from 0 to 11,990 cd/m^2 (average of all observations = 2997 cd/m^2, std.dev = 3011cd/m^2), and the global vertical illuminance at the lens ranged from 0 to 11,900 lux.

Results (presented in Figure 9 and Table 1) show that measurement accuracy was affected by both the magnitude of the change in global vertical illuminance during acquisition (Figure 9) and when the global vertical illuminance at the lens was very low (< 50 lux). When the global vertical illuminance at the lens was above 50 lux, the average error of the six cameras combined was 0.21%, with a standard deviation of 7.6%. Within this set of data, accuracy was shown to decrease when the change in global vertical illuminance during acquisition exceeded 5% (avg. error = 5.46% std. error = 13.59%), compared to when the change was less than 5% (avg. error = -0.21% std. error = 5.79%). When the global vertical illuminance at the lens was less than 50 lux (N = 67 images), the percent error of all cameras was significantly larger, however the magnitude error was not significant (avg. magnitude error = 8 cd/m^2, max magnitude error = 20 cd/m^2). Because this study focused on glare analysis, the small magnitude errors introduced by images acquired at global vertical illuminance levels below 50 lux were not considered a problem, and therefore images acquired under these conditions were retained.
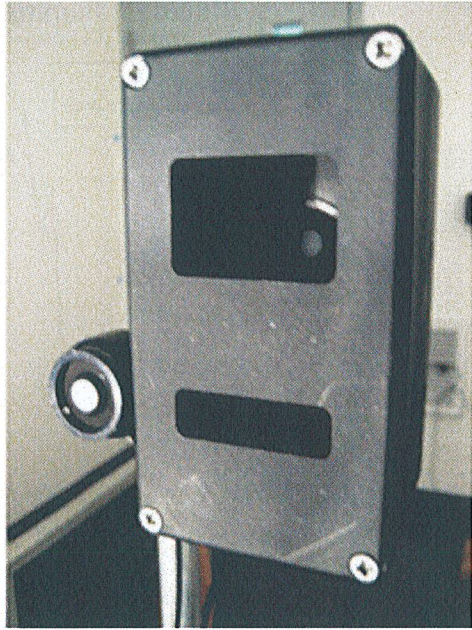
Figure 5. Illustration of the masked window region (left) that was compared to the equivalent region monitored by the shielded illuminance sensor (right).
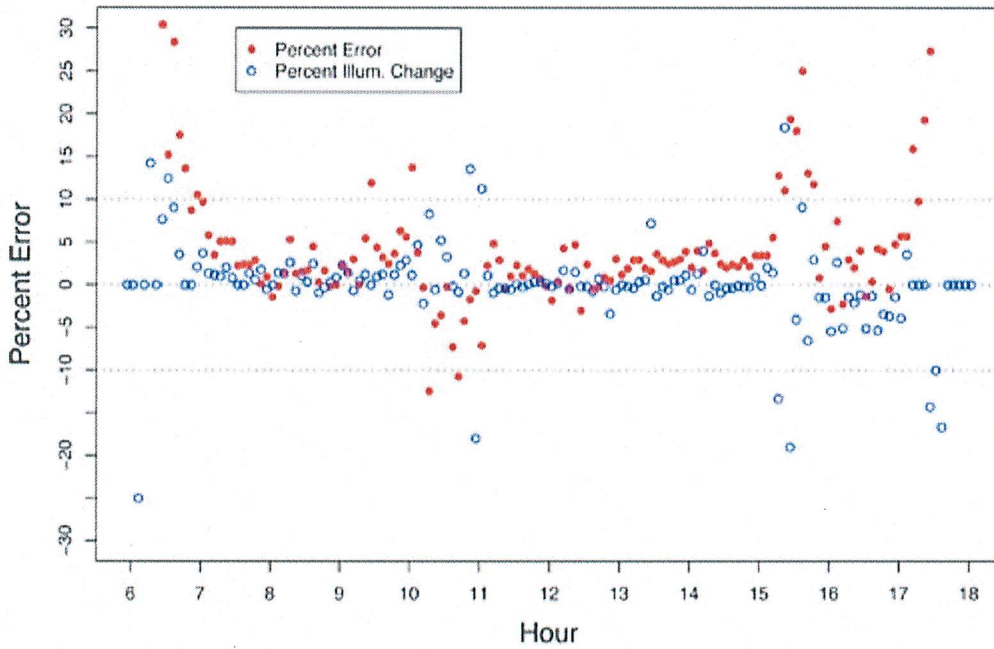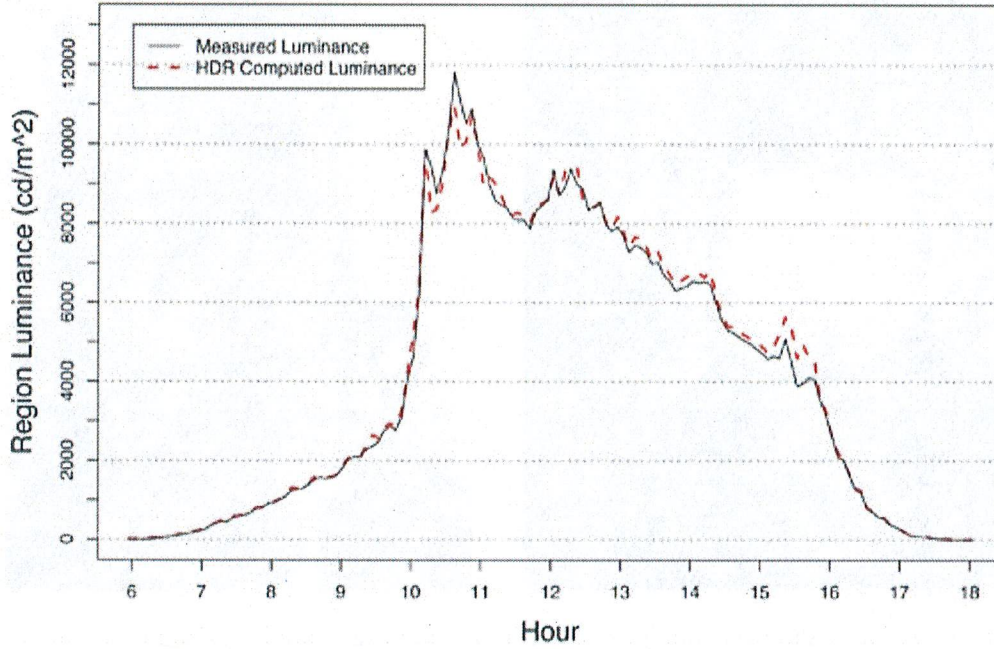
Figure 7. Comparison of window-region luminance derived from luminance maps versus a shielded illuminance sensor under dynamic sky conditions. Errors in excess of 30% occurred during low ambient lighting conditions and are not shown in the lower figure. All errors are summarized in Table 1.
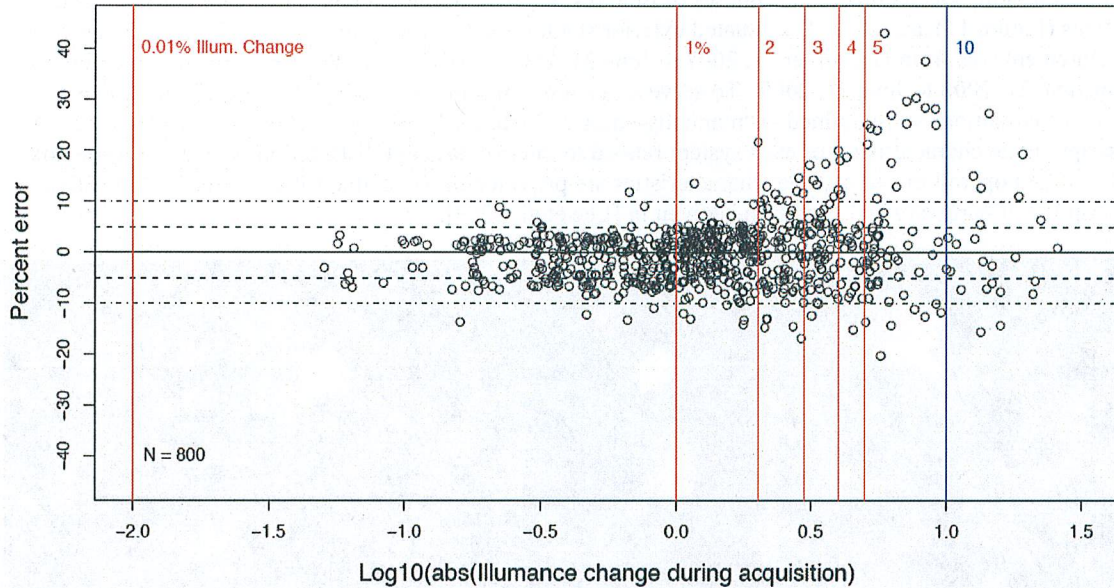
Figure 9. Illustration of the increasing magnitude of measurement errors as sky conditions (represented by change in vertical illuminance during acquisition) become increasingly unstable. This figure includes one day of image data (6 AM to 6 PM) for each of six cameras and does not include data acquired under low light levels (vertical illuminance < 50 lux).

Table 1. Measurement Errors During Unstable Sky Conditions.

Global vertical illuminance during acquisition	Camera Name	(All data)					Change in global vertical illuminance during acquisition (<= 5%)					Change in global vertical illuminance during acquisition (>5%)				
		N (images)	Avg % Error	SD % Error	Avg Magnitude Error (cd/m²)	SD Magnitude Error	N (images)	Avg % Error	SD % Error	Avg Magnitude Error (cd/m²)	SD Magnitude Error	N (images)	Avg % Error	SD % Error	Avg Magnitude Error (cd/m²)	SD Magnitude Error
> 50 lux	Av	130	-4.12%	5.39%	-59.2	47.7	119	-4.14%	4.72%	-59.8	48.2	11	-3.89%	10.58%	-52.8	42.52
	Aw	132	3.29%	7.36%	11.7	34.2	125	2.63%	5.50%	12	34.9	7	15.11%	19.58%	6	19.48
	Bv	133	-0.61%	7.22%	-76.7	303	118	-1.23%	6.23%	-77.8	294	10	7.14%	12.92%	-86.8	355.3
	Bw	133	3.98%	6.63%	71.6	273	114	3.26%	4.47%	73.4	214	11	7.31%	14.65%	5.36	528.1
	Cv	136	-2.92%	6.72%	-87	231	118	-3.05%	5.22%	-82.1	231	13	0.02%	14.29%	-57.5	96.15
	Cw	136	1.63%	8.64%	-46.4	807	121	1.28%	8.59%	-53.9	854	10	7.04%	9.50%	35.5	85.97
	All Cameras	800	0.21%	6.99%	-31	283	715	-0.21%	5.79%	-31.4	279	62	5.46%	13.59%	-25	187.9
< 50 lux	Av	15	168.62%	205.40%	5.33	3.39										
	Aw	14	266.54%	317.61%	9.14	5.91										
	Bv	10	223.05%	218.13%	8.5	2.92										
	Bw	10	180.59%	140.61%	11	3.92										
	Cv	10	162.58%	171.59%	6.9	5.22										
	Cw	8	127.30%	83.82%	10.5	2.56										
	All Cameras	67	188.11%	189.53%	8.56	3.99										

7

2.5. Test and Reference Conditions

Two, six month, solstice-to-solstice phases of field testing were defined. Phase I evaluated interior shading systems (Figure 11) and Phase II evaluated exterior shading systems (Figure 13). For Phase I, the period of measurement was from December 21, 2007 to June 21, 2008. For Phase II, the period of measurement was from June 21, 2008 to June 21, 2009. To serve as a simple benchmark to judge test conditions against, two reference conditions were defined: a "manually-adjusted" interior Venetian blind or fabric roller shade. A description the characteristics of each system related to interior daylight distribution is given in Appendix Table 1, and operation and material characteristics are provided in Appendix Tables 2 and 3. A detailed description of hardware and operation is given in [Lee et al. 2009].
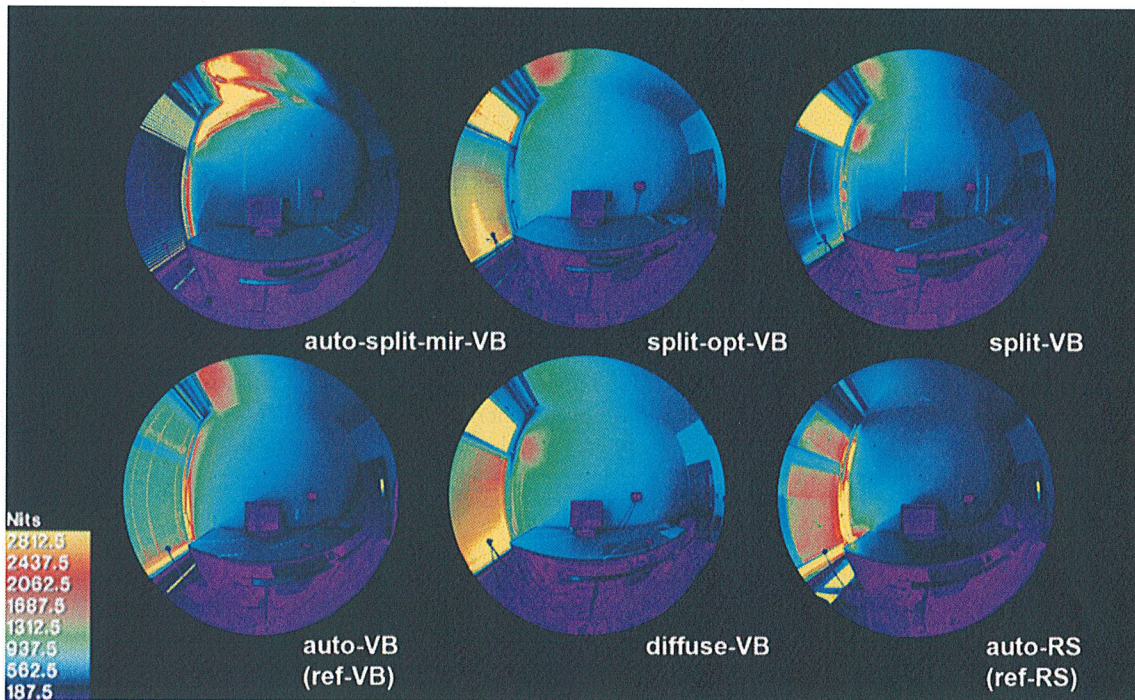

Figure 11. Phase I interior shade test conditions shown with falsecolor tone-mapping (yellow $\geq$ 3000 cd/m^2). The ref-VB was identical to the auto-VB, but seasonally adjusted to block direct sun. The ref-RS was identical to the auto-RS, but set at a fixed position 0.76 m (2.5 ft) above the floor.
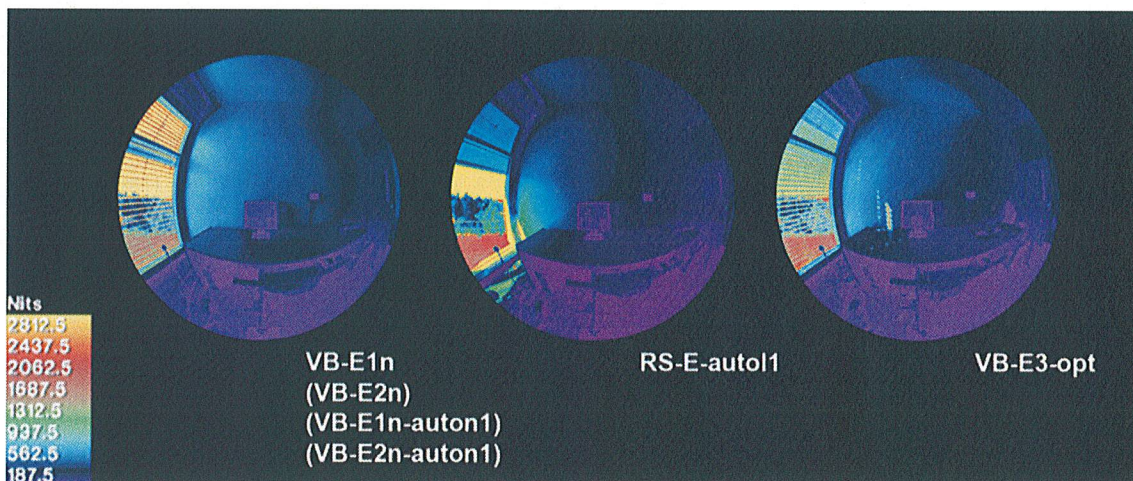

8

Figure 13. Phase II exterior shade test conditions shown with falsecolor tone-mapping (yellow $\geq$ 3000 cd/m^2). The VB-E2n, VB-E1n-auton, and VB-E2n-auton (indicated in parenthesis) are similar in appearance to the VB-E1n but involved either a more open upper region (E2), automation (auton1), or both.

2.6. Classification of sky conditions

Sky conditions were expected to have a significant influence on visual comfort outcomes
Therefore, a sky classification for each test day was determined using the method developed by [Darula and Kittler, 2004]. The classification is based on two parameters; the fraction of time, s, that the direct normal irradiation (measured using a pyroheliometer) exceeds 120 w/m^2, and U, the natural logarithm of the average of the absolute values of the change in global horizontal illuminance (lux) over a one-minute span. If s is less than 0.03, then conditions are considered to be overcast. If s is greater than or equal to 0.75, conditions are characterized as clear. For solar fractions between this range, if U is less than (10 - 6s), conditions are considered cloudy, otherwise they are considered dynamic. The resulting number of test days and sky conditions are summarized in Table 2.

Table 2 Summary of Phase I and Phase II sky conditions

Phase I

Test Condition	Orientation	Number of Days					Fraction of All Sky Conditions			
		N	clear	cloudy	dynamic	overcast	clear	cloudy	dynamic	overcast
auto-split-mir-VB	VDT	42	27	5	7	3	0.64	0.12	0.17	0.07
	window	45	30	5	7	3	0.62	0.13	0.18	0.08
auto-VB	VDT	16	10	1	4	1	0.62	0.06	0.25	0.06
	window	15	9	1	4	1	0.60	0.07	0.27	0.07
split-opt-VB	VDT	35	21	3	9	2	0.60	0.09	0.26	0.06
	window	35	21	3	9	2	0.60	0.09	0.26	0.06
split-VB	VDT	29	22	0	7	0	0.76	0.00	0.24	0.00
	window	31	21	0	7	3	0.68	0.00	0.23	0.10
diffuse-VB	VDT	26	19	1	4	2	0.73	0.04	0.15	0.08
	window	26	19	1	4	2	0.73	0.04	0.15	0.08
auto-RS	VDT	26	12	3	4	7	0.46	0.12	0.15	0.27
	window	26	13	3	4	6	0.50	0.12	0.15	0.23
						average	0.63	0.07	0.21	0.10

Phase II

Test Condition	Orientation	N	clear	cloudy	dynamic	overcast	clear	cloudy	dynamic	overcast
VB-E1n	VDT	45	30	2	7	6	0.67	0.04	0.16	0.13
	window	44	29	2	7	6	0.66	0.05	0.16	0.14
VB-E1n-auton1	VDT	76	31	9	22	14	0.41	0.12	0.29	0.18
	window	72	30	9	20	13	0.42	0.12	0.28	0.18
VB-E2n	VDT	33	22	2	8	1	0.67	0.06	0.24	0.03
	window	32	21	2	8	1	0.66	0.06	0.25	0.03
VB-E2n-auton1	VDT	24	14	3	4	3	0.58	0.12	0.17	0.12
	window	24	14	3	4	3	0.58	0.12	0.17	0.12
RS-E-auton1 (vs. ref-	VDT	49	28	5	13	3	0.57	0.1	0.27	0.06
	window	47	26	5	13	3	0.55	0.11	0.28	0.06
VB-E3opt	VDT	45	25	6	10	4	0.56	0.13	0.22	0.09
	window	45	25	6	10	4	0.56	0.13	0.22	0.09
RS-I-auto11	VDT	56	32	5	14	5	0.57	0.09	0.25	0.09
	window	47	29	3	13	2	0.62	0.06	0.28	0.04
						average	0.58	0.09	0.23	0.10

N varies for VDT and WIN views as a result of a varying errors in HDR acquisition between the two acquisition systems

3. IESNA region-based contrast ratio limits

The IESNA has developed guidelines for acceptable levels of non-uniformity expressed in terms of luminance ratios between surfaces in the field of view. The basis for the guideline is the physiological phenomenon called transient adaptation, a phenomenon associated with reduced visibility after viewing a higher or lower luminance than that of the task [IESNA 2005]. To avoid visual performance decrements, a maximum allowable contrast of [1:3:10] is permitted between the task, surroundings, and background.

Luminance maps are particularly well suited to the analysis of luminance ratios, as any number of arbitrarily shaped regions can be defined during analysis. In this study, regions were defined by creating a unique bitmap mask (Figure 15) and a process was implemented using *Radiance* to compute the average luminance for each of the masked regions. The visual task was defined as a visual display terminal (VDT) with a constant luminance of 200 cd/m^2, leading to discomfort thresholds of 600 cd/m^2 for "surrounding" regions (i.e., 1:3), and 2000 cd/m^2 for "background" regions (i.e., 1:10).

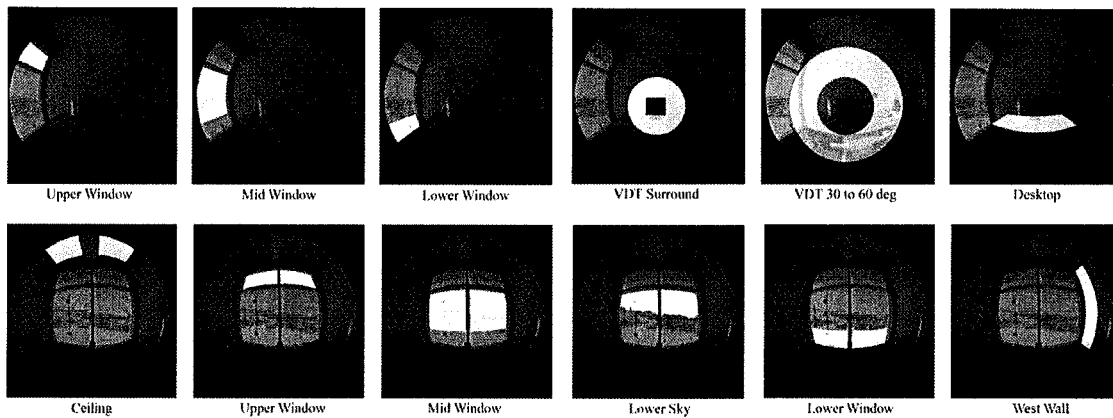| Upper Window | Mid Window | Lower Window | VDT Surround | VDT 30 to 60 deg | Desktop |
| Ceiling | Upper Window | Mid Window | Lower Sky | Lower Window | West Wall |

Figure 15. Illustration of the bitmap masks used to define regions in images acquired from the VDT-facing view point (upper row) and window-facing view point (lower row). For illustrative purposes, the bitmap mask (indicated in white) is superimposed on a generic image from each respective view orientation.

3.1. Analysis of region-luminance data

The analysis of region luminance data focused on differentiating between shading systems based on the frequency and degree of threshold exceedance produced by each pre-defined region. This method was used to evaluate 12 regions for each of 14 test conditions under four different sky conditions to quickly identify the regions and sky conditions that produced the greatest discomfort conditions.

As an example of this method (using Phase I data for the Window-facing orientation), Figure 17 illustrates the frequency and degree of threshold exceedance resulting from exceeding the IESNA recommended contrast ratio limits for the window regions under clear sky conditions. For each window region in Figure 17, there are two accompanying figures immediately below. The bottom figure indicates the percent of time (6 AM to 6 PM Standard Time) that the luminance threshold (2000 cd/m^2) was exceeded under all clear sky conditions. Data for all Phase I shading systems, including the reference conditions (indicated in brackets), are shown on the same plot (identified by a letter code).

As an indicator of the magnitude of threshold exceedance, the middle figure summarizes the distribution of values observed *above* the luminance threshold. The data are ordered and the first (Q1), second (Median) and third (Q3) quartiles are identified by horizontal lines. The median is indicated by a bold line within the box that is drawn around the inner quartile range (IQR). The whiskers extend to the smallest observation (i.e., 2001 cd/m^2) and largest observation (i.e., the maximum luminance recorded for that region).

This method enabled the identification of general trends in relative performance between systems, for example, the automated Venetian blind systems (A, B) controlled window luminance to within desired limits better than the static (i.e., seasonally adjusted) blind systems for all four regions (Figure 17). In addition, the method enabled the differentiation between systems based on the magnitude of "failure" conditions. As an example, the *upper window* region of the split-opt-VB, split-VB, and diffuse-VB test conditions resulted in significantly greater luminance levels when the luminance threshold was exceeded compared with other systems.

Finally, this method enabled the performance of individual systems to be assessed in greater detail spatially. For example, the performance of the split-opt-VB was better than the split-VB for the *upper* and *lower* window regions, but significantly worse for the *mid* and *lower sky* regions. The substantial variation in performance between regions (both within and across systems) illustrates the need for detailed analysis of innovative facade systems when the system is divided into different functional roles.
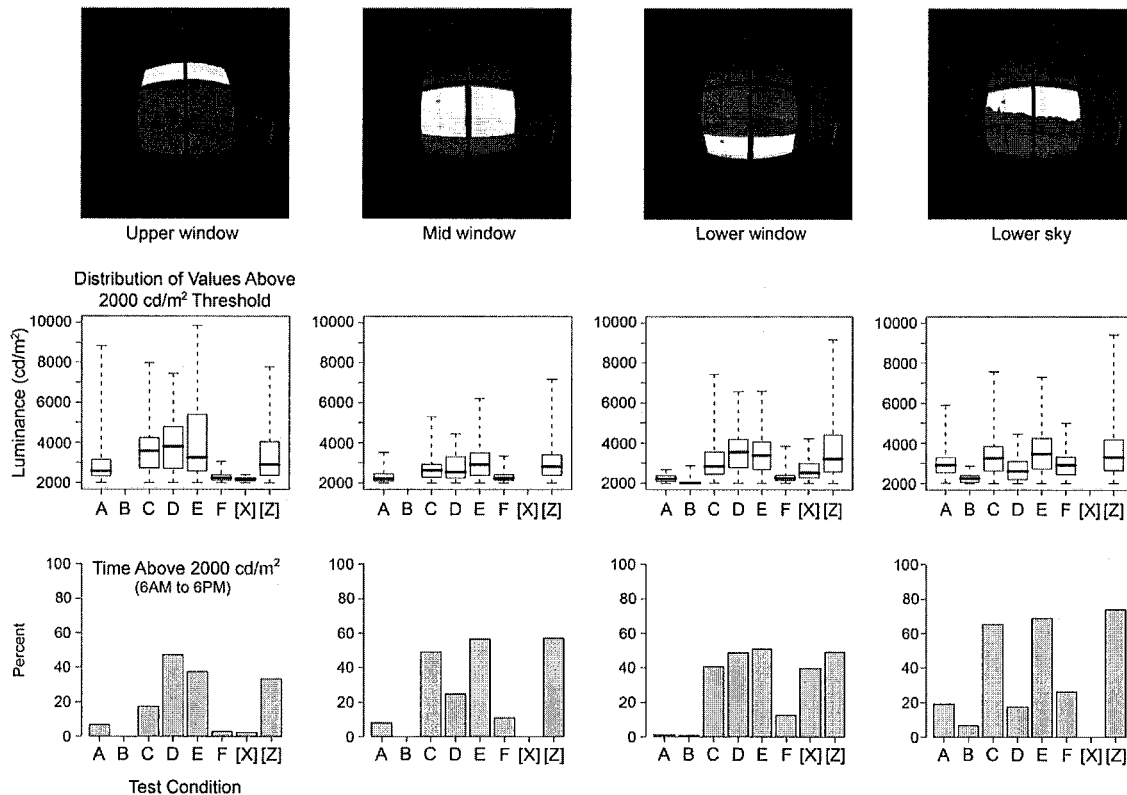

Figure 17. Summary of luminance values during clear sky conditions for Phase I test conditions (Window-facing orientation). A = auto-split-mir-VB (N = 27 days), B = auto-VB (N = 9), C = split-opt-VB (N = 19), D = split-VB (N = 20), E = diffuse-VB (N = 18), F = auto-RS (N = 12), [X] = ref-RS (N = 19), [Z] = ref-VB (N = 48).

4. The Daylight Glare Index

4.1. Discomfort Glare

The Hopkinson-Cornell large-source glare index (daylight glare index or DGI) is a metric commonly used to evaluate discomfort glare for large-area sources of glare such as windows [Hopkinson and Bradley, 1960; IES 1962]. DGI is computed from a formula that was developed to account for the effects of source brightness, size, location relative to line of sight, and adaptation luminance. Table 3 lists the mean subjective response to values from the DGI formula as measured in environments with windows.

$$DGI = 10\log 0.478 \sum_{i=1}^{n} \frac{L_s^{1.6} \cdot \Omega^{0.8}}{L_b + 0.07 \cdot \omega^{0.5} \cdot L_s} \tag{1}$$

where,

L_s Source luminance (cd/m^2)

L_b Background luminance (cd/m^2)

Ω Solid angular subtense of source modified for the effect of the observer in relation to the source (sr)

ω Solid angular subtense of source at the eye of the observer (sr)

Table 4. Subjective correlation to DGI

Glare Criterion	DGI
Just perceptible	16
Just acceptable	20
Just uncomfortable	24
Just intolerable	28

4.2. Detection of arbitrarily located glare sources

Although a luminance map provides a highly detailed representation of the visual environment, there remains the challenge of determining what regions in the image constitute a glare source in order to compute glare discomfort metrics such as the DGI. Addressing this issue is presently dealt with by specifying a threshold value for glare: either an absolute value (e.g., all sources above 1000 cd/m^2) or a ratio between a given pixel and the average luminance of the task or entire scene (e.g., 4:1). There is currently limited guidance for what this threshold value should be, or what method to use in order to represent the glare sensitivity of a human observer. In the development of *evalglare*, a tool to predict the probability of discomfort glare (DGP) from hemispherical luminance maps, Wienold and Christoffersen [2006] defined glare as any pixel four times greater in luminance than the average luminance of a circular visual task zone with an angle of ~0.53 sr. However, Wienold and Christoffersen did not indicate how the ratio of 4:1 was arrived at in favor of other possible ratios. *Evalglare* allows the user to select from multiple methods of glare detection (e.g., scene-based, task-based, and absolute) as well as specify the threshold. If the task-based method is chosen, the tool enables the user to define a circular task zone by specifying the centroid and solid angle.

In this study, glare sources were detected using the *Radiance* program *findglare* [Ward 1992]. The approach used by *findglare* to identify glare sources is called "thresholding," where the image is divided orthogonally into equal samples and if a particular sample is above a designated threshold value, then *findglare* assumes it must be part of a glare source. In this study a threshold value of 1000 cd/m^2 was used to detect glare sources. This value corresponds to a ratio of 5:1 relative to the task defined in this study (a VDT of average luminance = 200 cd/m^2). When a sample above the threshold value is found, it is merged with neighboring contiguous glare samples. Two glare samples are considered contiguous if they are separated by at most one non-glare sample. This allowed separation is to avoid the breakup of something like a window with Venetian blinds into an unreasonable number of sources. A glare source may have any number of holes in it and still be considered contiguous. The sample parameter was specified to generate a sample size of 2 pixels by 2 pixels, enabling the differentiation of glare sources located relatively close together. The output of *findglare* is the centroid, solid angle, and average luminance of each glare source identified. In this study, these values were then processed by another *Radiance* program *glarendx* to compute the DGI.

4.3. Weighting of Time-Series DGI Data

Because the DGI in a highly daylit space can cover a wide range of subjective values over the course of a day (from imperceptible up to uncomfortable or even intolerable glare), simple averaging of all observed values

can easily result in a summary value of "imperceptible" glare and therefore lead to misleading conclusions. There is no agreed upon procedure for handling this type of problem.

To address this problem, a weighted daylight glare index (DGI_w) sensitive to infrequent periods of perceptible-to-uncomfortable glare was implemented [Carmody 2004]. The weighting formula is relatively sensitive to extreme values of discomfort glare yet capable of discriminating between cases with single large excursions and cases with multiple but just slightly smaller excursions from the base value. The returned DGI_w value gives an average that is sensitive to excursions from a base value if they occur at a frequency of 1 percent or more and has a scale that is the same as that defined for an individual DGI value (e.g., 20 = "just noticeable", 22="just uncomfortable" etc.). We therefore constrained the minimum and maximum values of DGI and calculated a DGI_w from the constrained values for each day using the equation below. An example of the weighting method applied to 144 observations of the DGI is shown in Figure 19.

If DGI < 6, then set DGI to 6, or
if DGI > 32, then set DGI to 32,
else, $DGI_w = 4 * \log_{10} [\text{mean}(10^{(DGI/4)}]$ (2)
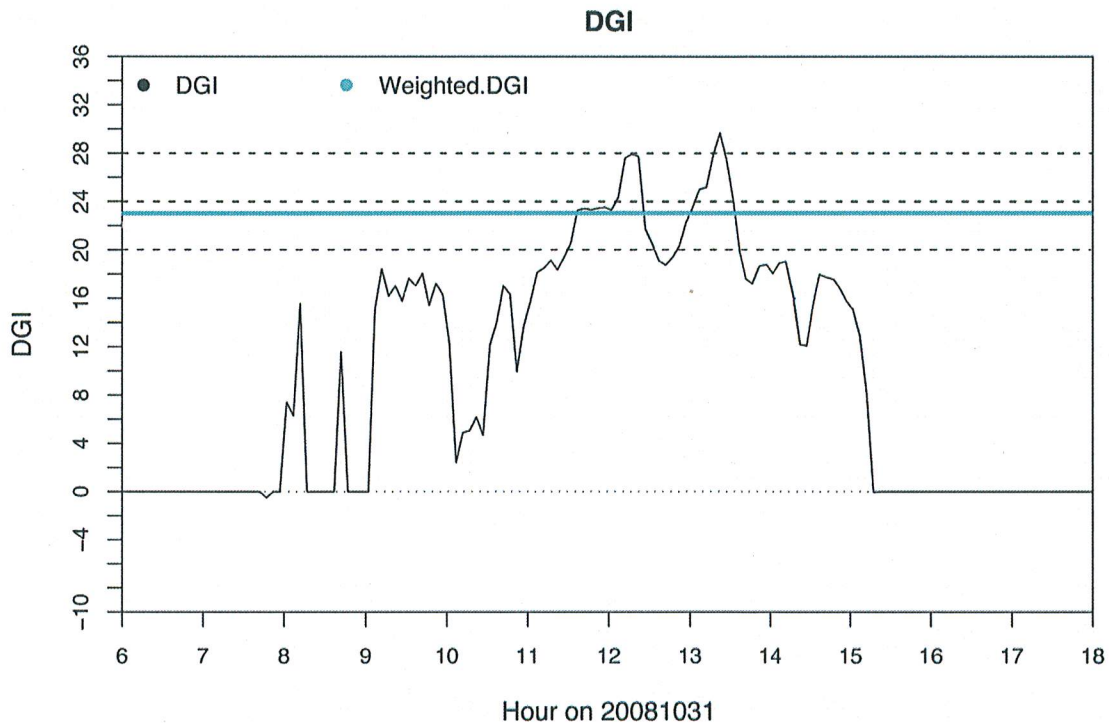where, DGI = Measured 5-min DGI data over the 12-h period from 6 AM to 6 PM.

Figure 19. Illustration of the dynamic variation of DGI data over one 12-h day and the corresponding DGI_w value (solid cyan line). The dotted horizontal lines correspond to the following semantic glare discomfort thresholds: 20 = "Just acceptable," 24 = "Just uncomfortable," 28 = "Just intolerable."

4.4. Analysis of DGI$_w$ Data

The DGI$_w$ analysis focused on two goals 1) differentiating system performance across seasonal variation in sun and sky conditions and 2) providing an "overall" summary of visual comfort performance for the solstice-to-solstice interval. Although the DGI$_w$ analysis indicated discomfort conditions under non-clear sky conditions, the unequal number of sky conditions recorded for each system combined with the uneven distribution of non-clear conditions throughout the test intervals resulted in the analysis focusing on clear sky data.

Using the auto-split-mir-VB as an example, Figure 21 illustrates both the daily and seasonal variability of time-series DGI data that was recorded for clear sky conditions during Phase I testing. For each day (indicated on the x-axis in MMDD format) the 5-minute time-series DGI data is plotted on the y-axis and color-coded by magnitude of discomfort (e.g., yellow corresponds to "just uncomfortable"). The green lines indicate the times when seasonal slat adjustments were made to the ref-VB. This graphic technique enables one to visualize the time and magnitude of visual discomfort for each test condition and provided feedback to improve the operation of dynamic systems by indicating specific times for more detailed diagnostics.
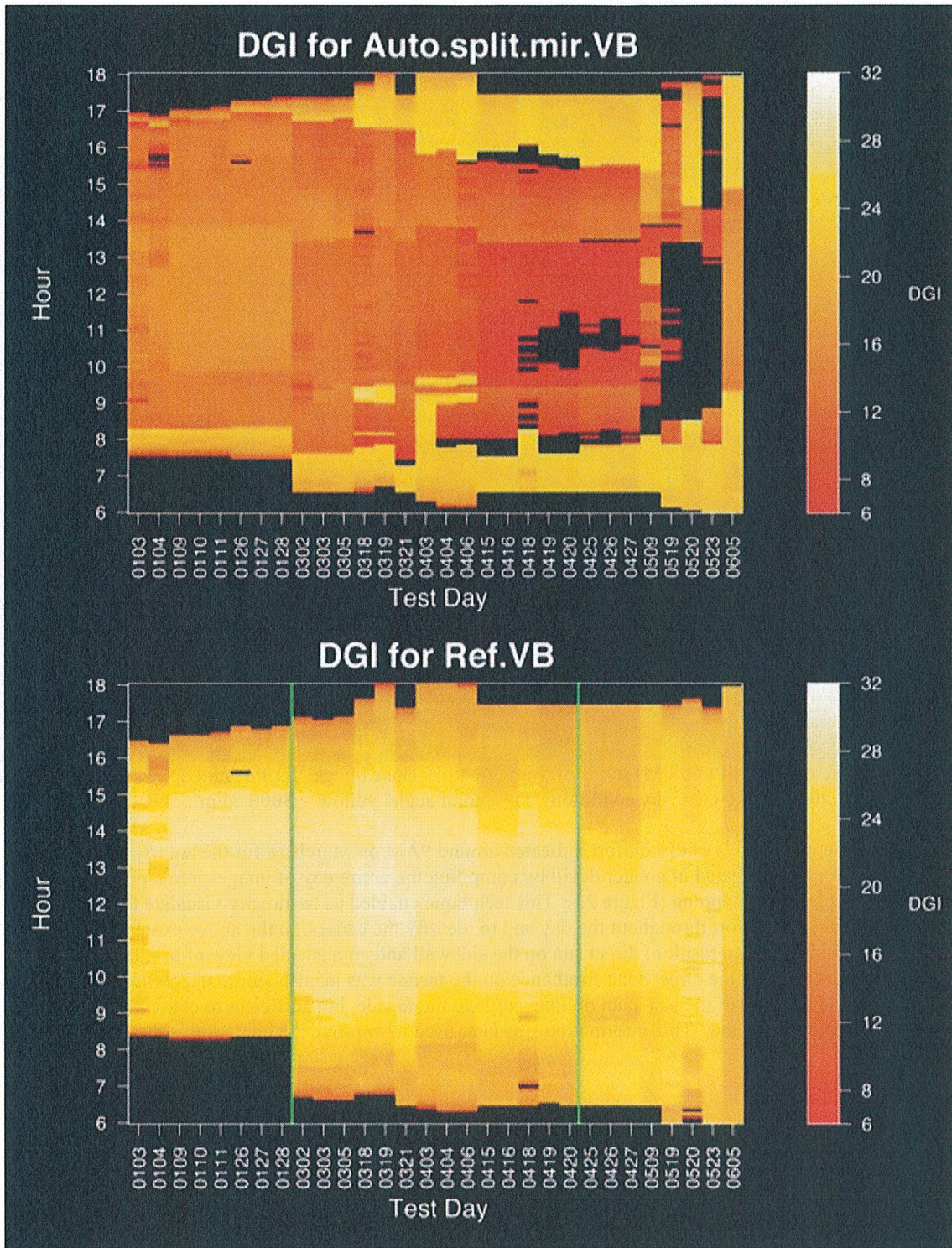
14

Figure 21. Side-by-side comparison of the auto-split-mir-VB versus the ref-VB under simultaneous exterior solar conditions. Issues related to image acquisition resulted in missing data on some days in the early morning (6 AM to 6:30 AM) and evening (5:30 PM to 6 PM) Standard Time. The vertical green lines indicate the times when seasonal slat adjustments were made to the ref-VB.
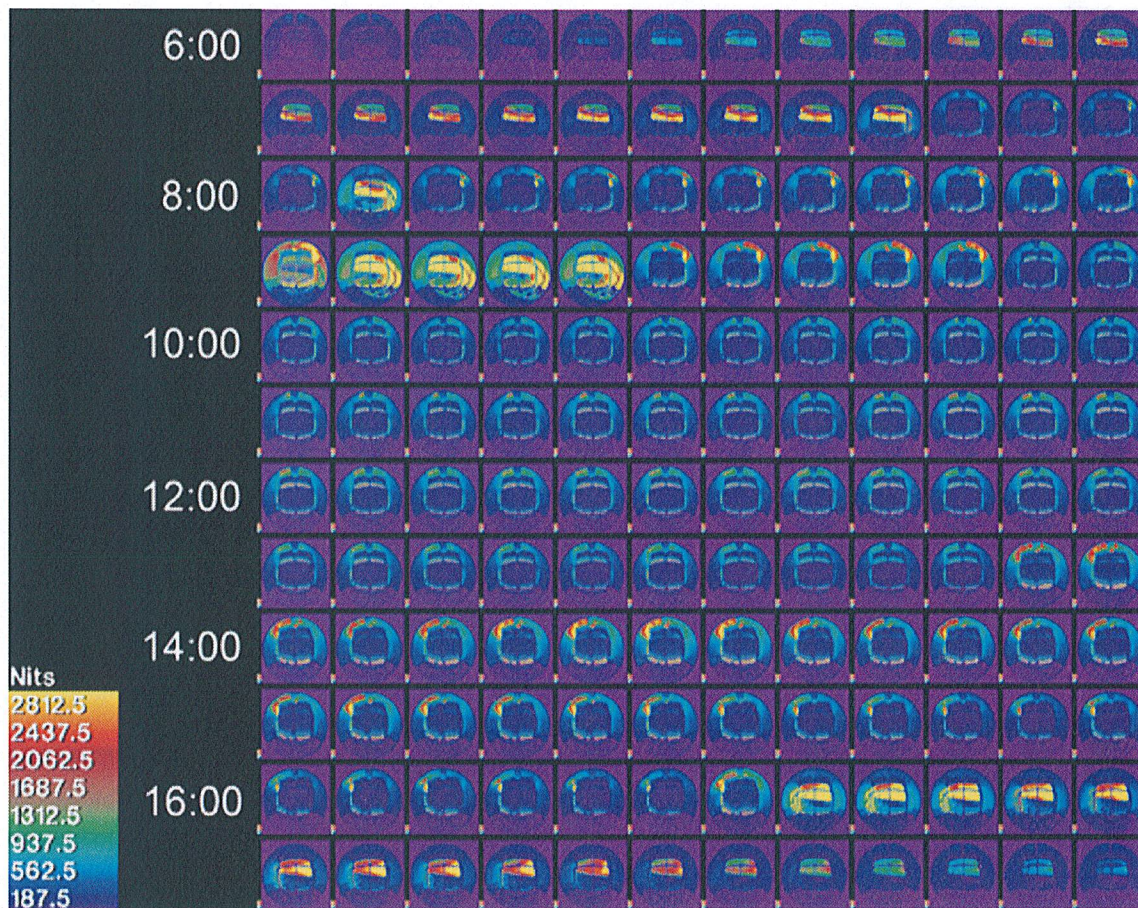
Figure 23. One day (6 AM to 6 PM) series of 5-minute time-lapse images for the auto-split-mir-VB acquired on March 18, 2010 during clear sky conditions. Falsecolor scale: yellow $\geq$ 3000 cd/m^2.

As an example, the periods of discomfort indicated around 9AM on March 18 for the auto-split-mir-VB (Figure 21) were investigated in greater detail by compiling the entire day of images into a time-lapse movie using a falsecolor tone-mapping (Figure 23). This technique enabled us to directly visualize the scenes that resulted in glare discomfort throughout the day and to identify the causes. In the above example (Figure 23), the glare discomfort was a result of direct sun on the sidewall and an unshaded view of bright sky. These conditions existed while the direct solar irradiance on the facade was insufficient to trigger the deployment of the blind due to position of the sun at an oblique angle to the facade, but sufficient to cause discomfort for an unacceptable period of time. This information was later used to improve the control algorithm used to control this system.
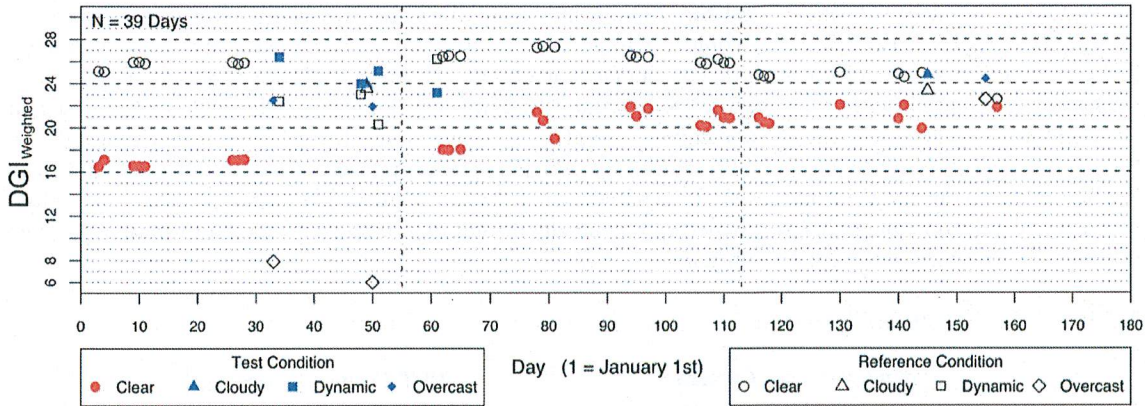
Figure 24. Plot of DGI$_w$ values for Phase I testing of the auto-split-mir-VB paired against the ref-VB (window-facing orientation). Values are coded by Darula sky classification. Only clear days (red dots) were used in the summary analysis. The vertical lines indicate the times when seasonal slat adjustments were made to the ref-VB.

Figure 24 illustrates the seasonal distribution of DGI$_w$ values for the auto-split-mir-VB and ref-VB pairing. In this figure, DGI$_w$ values for non-clear sky conditions are included for illustrative purposes. The increasing trend in DGI$_w$ values from winter to summer reflects the increasing periods of visual discomfort in the morning and evening (indicated in yellow in Figure 9) that occurred as the system remained retracted until the exterior vertical illuminance threshold was exceeded and the blind deployed.
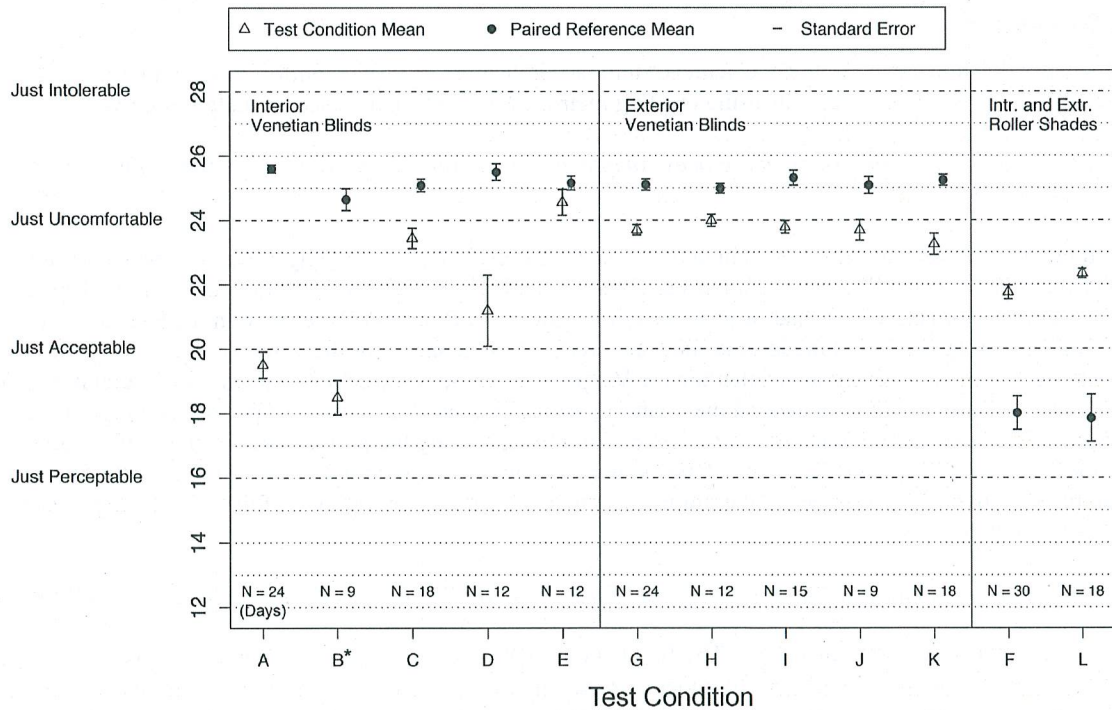
Figure 25. Plot of the mean and standard error of DGI$_w$ values for each interior and exterior test condition (x-axis) compared against its reference condition (y-axis) for the window-facing orientation during clear sky conditions.

Figure 25 summarizes the DGI$_w$ values for Phase I and II shading systems for the window-facing orientation under clear sky conditions. The summary was created by taking the average of the DGI$_w$ values over the

17

solstice-to-solstice interval for each test condition, using an equal number of test days from each interval of seasonal slat-angle adjustment (e.g., "winter, "equinox," "summer") to not bias the results toward a system that performed better or worse during one particular time of year. The standard error is provided as an indicator of the variability in the observed DGI_w values. Data for this figure and letter-code for each system are given in Table 5. All results include equal groups of test days from each third of the solstice-to-solstice test interval except for test condition "B" (auto-VB), which due to operational issues, resulted in 2 test days in the first third, no days in the middle, and 7 days in the final third. Because glare conditions were generally more severe at lower sun angles, it is expected that an equal sampling of test days would result in a greater summary DGI_w score for this test condition.

Table 5. Summary of DGI_w data

Test Condition	Code	Window-Facing Camera					VDT-Facing Camera				
		N	Mean.test	SE.test	Mean.ref	SE.ref	N	Mean.test	SE.test	Mean.ref	SE.ref
auto-split-mir-VB	A	24	19.5	0.41	25.6	0.12	21	11.9	0.27	13.5	0.36
auto-VB	B	9	18.5	0.53	24.6	0.34	10	7.2	0.19	12.3	0.50
split-opt-VB	C	18	23.4	0.32	25.1	0.20	18	12.2	0.32	13.2	0.40
split-VB	D	12	21.2	1.11	25.5	0.26	12	10.3	0.52	13.5	0.57
diffuse-VB	E	12	24.6	0.40	25.2	0.21	12	13.8	0.42	13.2	0.47
VB-E1n	G	24	23.7	0.16	25.1	0.17	21	11.9	0.27	13.5	0.36
VB-E1n-auton1	H	12	24.0	0.19	25.0	0.15	12	11.6	0.27	13.4	0.29
VB-E2n	I	15	23.8	0.20	25.3	0.23	18	12.8	0.36	13.6	0.40
VB-E2n-auton1	J	9	23.7	0.32	25.1	0.26	9	12.6	0.74	13.8	0.65
VB-E3opt	K	18	23.2	0.33	25.2	0.17	18	12.3	0.33	13.5	0.31
RS-I-auto11	F	30	21.8	0.22	18.0	0.52	33	13.2	0.27	10.2	0.43
RS-E-auton1	L	18	22.3	0.14	17.9	0.73	18	13.7	0.89	10.0	0.62

5. Discussion

This paper illustrates two methods to achieve summary indicators of visual comfort based on performance over solstice-to-solstice conditions using existing metrics. The analysis focused on addressing two questions:

1) *Do existing metrics and summary indices computed from luminance maps enable differentiation between systems?*

Both methods enabled general trends in performance between groups of shading systems to be identified and these trends were generally consistent between the two methods. For example, of all Venetian blind systems tested, the interior automated shading systems (auto-split-mir-VB, auto-VB) resulted in the lowest summary DGI_w scores (Figure 25) and the least luminance threshold exceedance for the window regions (Figure 17). In addition, both methods indicated that the ref-VB performed the worst of all systems tested, with the highest DGI_w score (Figure 25) and in general the greatest periods of exceedance for most pre-defined regions (Figure 17). However, the methods were not consistent in assessing the performance of the static interior subdivided systems (split-opt-VB, split-VB), where the split-VB resulted in a lower summary DGI_w score than the split-opt-VB, yet exceeded the luminance threshold for a greater period of time for the *upper* and *lower* window regions.

2) *What value can time-lapse imaging add over more conventional methods of visual comfort assessment?*

Two benefits were found in this study. The first benefit, demonstrated in Section 3, is the ability to subdivide regions of the image into an arbitrary number of zones of any arbitrary shape. This capability enabled us to differentiate performance between systems with greater spatial detail. For example, the performance of the split-opt-VB was better than the split-VB for the *upper* and *lower* window regions, but significantly worse for the *mid* and *lower sky* regions (Figure 17). The substantial variation in performance between regions (both within and across systems) illustrates the need for detailed analysis of innovative facade systems when the system is divided into different functional roles.

The second and perhaps more significant benefit is that an HDR image can be used to directly visualize the magnitude and distribution of light throughout the day. Used primarily as a diagnostic technique in this study, daily sets of HDR images compiled into time-lapse movies enabled the performance of dynamic shading and light redirecting systems to be evaluated and improved by visually identifying the conditions that caused discomfort (Figure 23).

6. Conclusions

Six-month, solstice-to-solstice experimental tests were conducted of both conventional and innovative interior and exterior shading systems on south-facing, large-area windows at a full-scale daylight test facility, located in a predominantly sunny climate in Berkeley, California. These systems used a variety of strategies, including optics, subdivision of the window wall into a lower view and upper daylighting zone, and automated controls, with the goal of achieving a more balanced and comfortable luminous environment.

The objective of this study was to explore how calibrated high dynamic range (HDR) images (luminance maps) acquired in real world daylit environments can be used to characterize, evaluate, and compare visual comfort conditions of innovative facade shading and light-redirecting systems. Detailed (1536 x 1536 pixel) luminance maps were time-lapse acquired at 5-min intervals over a 12-h period from two view positions in an unoccupied full scale testbed facility. These luminance maps were analyzed using a weighted Hopkinson Cornell Daylight Glare Index (DGI) and the IESNA recommended contrast ratio limits to quantify how innovative interior and exterior shading systems compared to conventional systems under real sun and sky conditions over a solstice-to-solstice test interval. Glare sources for the DGI calculation were detected using the Radiance *findglare* tool assuming a threshold value of 1000 cd/m^2. Contrast ratios were based on the luminance of user-defined masked regions of the luminance map, assuming a computer-based task with a visual display terminal (VDT) average luminance of 200 cd/m^2.

Based on the results of this study, the following conclusions were made:

1. Both the weighted DGI and the IESNA recommended contrast ratio limits enabled general trends in performance between groups of shading systems to be identified and these trends were generally consistent between the two indicators.

2. Compared to existing methods of analysis that define the entire window as a single glare source, luminance maps indicate that the magnitude and duration of visual discomfort varied significantly for many systems across the "masked" regions defined for the window and illustrate the need for more detailed spatial analysis when assessing the visual comfort performance of innovative facade systems.

3. Daily sets of luminance maps compiled into movies with a false-color tone-mapping can provide a significant advantage over conventional visual discomfort indicators when used as a diagnostic technique to visualize, assess, and improve the performance of control algorithms for automated shading and light redirecting systems.

Luminance maps, corrected for lens light fall off (vignetting) and calibrated against an adjacent illuminance sensor, are reasonably accurate on average under dynamic sky conditions when the change in global vertical illuminance during acquisition is below 5% (avg. % error of the six cameras = -0.21%, standard deviation = 5.79%, N = 715 images). However, luminance data becomes significantly less accurate when the change in global vertical illuminance at the lens during acquisition exceeds 5% (avg. % error of the six cameras = 5.46%, standard deviation = 13.59%, N = 62 images).

References

Carmody J, Selkowitz SE, Lee ES, Arasteh D, Willmert T. 2004. Window systems for high-performance buildings. W.W. Norton & Co. New York, London, 362-363.

Clear RD, Inkarojrit V, Lee ES. 2006. Subject responses to electrochromic windows. Energy and Buildings. 38(7): 758-779.

Darula S, Kittler R. 2004. Sunshine duration and daily courses of illuminance in Bratislava. International Journal of Climatology 24: 1777-1783.

Debevec PE, Malik J. 1997. Recovering high dynamic range radiance maps from photographs. SIGGRAPH, 369-378.

Fan D, Mardaljevic J. 2009. HDRcapOSX. How to automate capture using a Mac Mini less k/b and screen. <http://www.iesd.dmu.ac.uk/~jm/doku.php?id=resources:hdrcaposx> Accessed 2011 10 Jan.

Hopkinson RG, Bradley RC. 1960. "Glare from very large sources", Illuminating Engineering, 55, 288-297.

Hopkinson RG. 1972. "Glare from daylighting in buildings", Applied Ergonomics, 3, 206-215.

Aschehoug O, Christoffersen J, Jakobiak R, Johnsen K, Lee ES, Ruck N, Selkowitz SE, editors. 2000. Daylight In Buildings: A source book on daylighting systems and components. A Report of IEA SHC Task 21 / ECBCS Annex 29.

Rea M, editor. 2000. The IESNA Lighting Handbook. 9th ed. New York: The Illuminating Engineering Society of North America. Luminance ratio limits; ch. 11, pp. 16-18.

Inanici M, Galvin J. 2004. Evaluation of high dynamic range photography as a luminance mapping Technique. Lawrence Berkeley National Laboratory. <http://escholarship.org/uc/item/9h61f5h8> Accessed 2011 10 Jan.

Lee ES., Selkowitz SE, DiBartolomeo DL, Klems JH, Clear RD, Konis K, Hitchcock R, Yazdanian M, Mitchell R, Konstantoglou M. 2009. *High performance building facade solutions.* California Energy Commission, PIER. Publication number CEC-500-06-041.

Mitsunaga T, Nayar SK. 1999. IEEE Conference on computer vision and pattern recognition (CVPR), Vol.1, 374-380.

Nabil A, Mardaljevic J. 2006. Useful daylight illuminances: A replacement for daylight factors. Energy and Buildings. 38(7): 905-913.

Sutter Y, Dumortier D, Fontoynont M. 2006. The Use of shading systems in VDU task offices: A pilot study. Energy and Buildings 38(7): 780-789.

Tuaycharoen N, Tregenza PR. 2007. View and discomfort glare from windows. Lighting Research and Technology. 39(2): 185-200.

U.S. Green Building Council. 2009. LEED 2009 for new construction and major renovations rating system. Version 3.

Ward G. 1991. Real Pixels. Graphics Gems II, edited by James Arvo, Academic Press.

Ward G. 1994. The RADIANCE Lighting Simulation and rendering system. Computer Graphics (Proceedings of Siggraph 94).

Ward G. 1992. Radiance Visual Comfort Calculation.
<http://radsite.lbl.gov/radiance/refer/Notes/glare.html> Accessed 2011 10 Jan.

Wienold J, Christoffersen J. 2006. Evaluation methods and development of a new glare prediction model for daylight environments with the use of CCD cameras. Energy and Buildings. 38(7): 743–757.

APPENDIX

Appendix Table 1. Summary of Phase I and Phase II test and reference conditions

Phase I: Interior Test Conditions	Code	Daylighting / Control Strategy
Automated, split optical venetian blind	auto-split-mir-VB	Scheduled slat adjustment to block direct sun and redirect daylight to the ceiling and upper wall regions. Retracted when exterior vertial illuminance decreased below fixed value.
Automated, matte-white venetian blind	auto-VB	Automated slat adjustments to regulate daylight transmission in response to workplane illuminance and exterior solar conditions.
Manually-operated, optical venetian blind	split-opt-VB	Reflective slats with a prismatic function to redirect daylight onto the ceiling and upper wall regions.
Manually-operated, split venetian blind	split-VB	Semi-gloss white coating on top surface of slats to diffussly reflect incident daylight. Lower surface is brushed silver with low-e
Automated, fiberglass/PVC fabric roller shade	auto-RS	Automated height adjustments to limit daylight penetration to a depth of 0.91 m (3 ft) from the interior face of glazing.
Translucent diffusing panel and manually-operated venetian blind	diffuse-VB	Ttranslucent panel (VLT ~30%) in upper window region. Lower section identical to the reference-VB.

Phase II: Exterior Test Conditions		
Manually-operated, full height venetian blind	VB-El n	2" slats with semi-gloss white coating adjusted seasonally to block direct sun and diffusly reflect daylight.
Automated, full-height venetian blind	VB-El n-auton1	Identical to the VB-El n, but automated based on a manufacturer's schedule to block direct sun, resulting in two tilt adjustments/day.
Manually-operated, full height two-zone venetian blind	VB-E2n	Zoned version of the VB-El n. The upper zone was set at a more open position relative to the lower zone to increase daylight
Automated, full-height two-zone venetian blind	VB-E2n-auton1	Identical to the VB-E2n, but automated based on a manufacturer's schedule to block direct sun, resulting in two tilt adjustments each
Manually-operated, three-zone mirrored horizontal louver system	VB-E3opt	Upper region blocking direct view of the sky, middle and lower allow increasing levels of daylight transmission and view to the
Automated, fabric roller shade	RS-E-autol1	Exterior version of auto-RS.

Reference Conditions		
Seasonally-operated interior venetian blind	Reference-VB	Slat angle adjusted at two-month intervals to block direct sun for the majority of the day.
Static fabric roller shade	reference-RS	Set at a fixed height of 0.76 m (30 inch) above the floor for the duration of testing.

Appendix Table 2. Description of Venetian blind systems

Shade type	Zone	Slat concave	Slat width (mm)	Slat width (in)	Slat spacing (mm)	Slat spacing (in)	Slat top surface	Slat bottom surface	Upper+lower slats ganged?
Interior Systems									
reference-VB	none	down	25.4	1.0	20.0	0.79	semi-gloss white	semi-gloss white	no
split-VB	upper	down	25.0	1.0	20.0	0.79	semi-gloss white	reflective metal	yes
	lower	down	25.0	1.0	20.0	0.79	white	reflective metal	yes
split-opt-VB	upper	up	25.0	1.0	17.0	0.67	matte white	prism	no
	lower	up	25.0	1.0	17.0	0.67	prism	matte white	no
auto-split-mir-VB	upper	up	82.5	3.2	71.4	2.81	mirror	matte gray	yes
	lower	up	82.5	3.2	71.4	2.81	shiny white	matte gray	yes
auto-VB	none	down	25.4	1.0	20.0	0.79	matte white	matte white	no
diff-VB	lower	down	25.4	1.0	20.0	0.79	semi-gloss white	semi-gloss white	no
Exterior Systems									
VB-E1n, VB-E1n-auton1	none	down	100.0	3.94	85.0	3.35	semi-gloss white	semi-gloss white	no
VB-E2n, VB-E2n-auton1	upper	down	100.0	3.94	85.0	3.35	semi-gloss white	semi-gloss white	no
	lower	down	100.0	3.94	85.0	3.35	semi-gloss white	semi-gloss white	no
VB-E3opt	upper	down	77.0	3.03	70.0	2.76	polished aluminium	matte light gray	yes
	middle	down	77.0	3.03	70.0	2.76	polished aluminium	matte light gray	yes
	lower	down	77.0	3.03	70.0	2.76	polished aluminium	matte light gray	yes

Appendix Table 3. Operation of Venetian blind systems

Shade type	Zone	Operation	Auto?	SA winter (deg)	SA equinox (deg)	SA summer (deg)	BA winter (deg)	BA equinox (deg)	BA summer (deg)	Height above floor (m)
Interior Systems										
reference-VB			no	58	12	0	0	30	35	0
split-VB	upper		no	35	10	0	20	35	35	0
	lower		no	55	34	28	0	16	20	0
split-opt-VB	upper		no	28	6	0	20	35	35	0
	lower		no	50	12	0	0	30	35	0
auto-split-mir-VB	upper	early AM late PM	yes	15	5	0	20	35	30	0, 2.74
	lower	early AM late PM	yes	75	63	54	0	0	2	0, 2.74
	upper	10:00-14:00	yes	28	28	8	6	6	25	0, 2.74
	lower	10:00-14:00	yes	78	78	70	0	0	0	0, 2.74
auto-VB			yes LBNL control of slat angles							0
diff-VB	lower		no	58	12	0	0	30	35	0
Exterior Systems										
VB-E1n			no	56	16	16	4	32	32	0
VB-E2n	upper		no	31	16	16	22	32	32	0
	lower		no	56	16	16	4	32	32	0
VB-E1n-auton1			yes Manufacturer control of slat angles: solar exclusion							0
VB-E2n-auton1	upper		yes Manufacturer control of slat angles: daylight							0
	lower		Manufacturer control of slat angles: solar exclusion							0
VB-E3opt	upper		no	63	63	63	4	4	4	0
	middle		no	36	36	36	20	20	20	0
	lower		no	17	17	17	31	31	31	0

Positive slat angle: Occupant can see the exterior ground from the interior.
Auto: automated; SA: slat angle; BS: blocking angle; deg: degrees
Blocking angle is defined as the profile or cut-off angle between two slats at normal incidence to the glass.
Slat angle was defined as the angle between horizontal and the plane defined by the two outside edges of the slat.